THE JOURNAL OF PHYSICAL CHEMISTRY LETTERS
A JOURNAL OF THE AMERICAN CHEMICAL SOCIETY

pubs.acs.org/JPCL

Letter

Coordination of Redox Ions within a Membrane-Binding Peptide: A Tale of Aromatic Rings

Riqiang Fu,* Mary T. Rooney, Rongfu Zhang, and Myriam L. Cotten*

Cite This: *J. Phys. Chem. Lett.* 2021, 12, 4392–4399

Read Online

ACCESS | Metrics & More | Article Recommendations | Supporting Information

ABSTRACT: The amino-terminal-copper-and-nickel-binding (ATCUN) motif, a tripeptide sequence ending with a histidine, confers important functions to proteins and peptides. Few high-resolution studies have been performed on the ATCUN motifs of membrane-associated proteins and peptides, limiting our understanding of how they stabilize Cu^{2+}/Ni^{2+} in membranes. Here, we leverage solid-state NMR to investigate metal-binding to piscidin-1 (P1), a host-defense peptide featuring F1F2H3 as its ATCUN motif. Bound to redox ions, P1 chemically and physically damages pathogenic cell membranes. We design $^{13}C/^{15}N$ correlation experiments to detect and assign the deprotonated nitrogens produced and/or shifted by Ni^{2+}-binding. Occupying multiple chemical states in P1-apo, H3 and the neighboring H4 respond to metalation by populating only the τ-tautomer. H3, as a proximal histidine, directly coordinates the metal, compared to the distal H4. Density functional theory calculations reflect this noncanonical arrangement and point toward cation−π interactions between the F1/F2/H4 aromatic rings and metal. These structural findings, which are relevant to other ATCUN-containing membrane peptides, could help design new therapeutics and materials for use in the areas of drug-resistant bacteria, neurological disorders, and biomedical imaging.

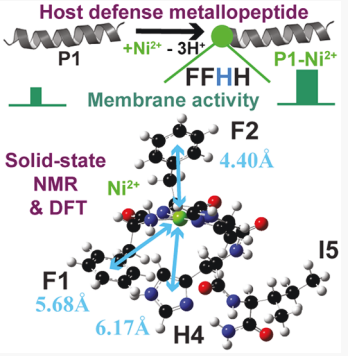

A broad range of vital biological processes depend on the concerted actions of metal ions coordinated to peptides and proteins.[1−6] In this context, the amino-terminal-copper-and-nickel-binding (ATCUN) motif has garnered much interest due to its advantages as a framework to investigate existing functions and engineer new ones.[6−11] Advantageous redox and nonredox functions of the ATCUN motif include its ability to cleave/modify proteins, nucleic acids, and lipids, sequester and transport metal ions, and act as a spectroscopic probe and imaging agent.[1,8−12] The ATCUN motif binds Cu^{2+}/Ni^{2+} via four nitrogens from a tripeptide sequence ending with histidine, a ubiquitous metal chelator (Figure 1a). It has been studied mostly in the context of water-soluble proteins, with the main structural features obtained by applying X-ray to model tripeptides.[7−14] Thus, little is known about the overall structural arrangement of the ATCUN motif in membrane-bound peptides/proteins, limiting our knowledge of how these overcome the energy cost of burying metal ions in hydrophobic membranes, especially if they lack tertiary structure to shield the metal ion. A possible source of stabilization could be electron-rich rings from aromatic side chains since they can both engage in favorable cation−π interactions[15−18] and facilitate the anchoring of membrane proteins/peptides at the water−bilayer interface.[19−23]

Here, we leverage solid-state NMR to investigate metal coordination to piscidin-1 (P1, FFHHIFRGIVHVGKTIHRLVTG), a membrane-binding ATCUN-containing host-defense peptide (HDP) rich in aromatic residues.[24,25] HDPs are promising templates for the development of novel anti-

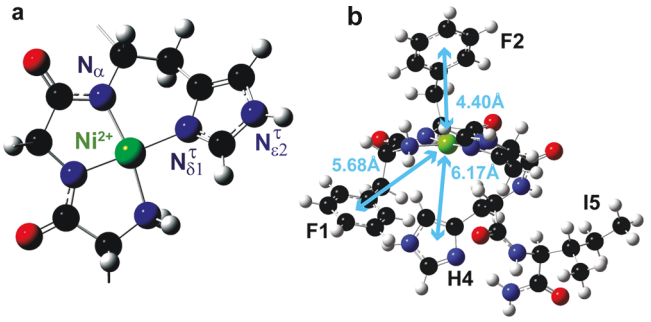

Figure 1. DFT-optimized ATCUN motif of P1 bound to Ni^{2+}. (a) F1F2H3, the ATCUN motif at the N-terminus of P1, is shown. Structurally, Cu^{2+}/Ni^{2+}-coordination occurs in a square planar geometry, with bonding to four nitrogen ligands: three backbone nitrogens and the $N_{\delta 1}$ of H3 (b) FFHHI, an extended ATCUN motif within P1, is displayed. The four nitrogen ligands, including the H3 side chain, sit in the plane perpendicular to the figure. F1, F2, and H4 form a cluster of aromatic rings close enough to Ni^{2+} to interact via cation−π interactions. Distances between Ni^{2+} and aromatic ring centers appear in blue. The coloring scheme is carbon (black), oxygens (red), nitrogen (blue), Ni^{2+} (green).

Received: February 27, 2021
Accepted: April 29, 2021
Published: May 3, 2021

https://doi.org/10.1021/acs.jpclett.1c00636
J. Phys. Chem. Lett. 2021, 12, 4392−4399

infective therapeutics to fight antibiotic resistance and boost immunity.[26−33] Bound to Cu^{2+}, P1 forms radicals that oxidize unsaturated fatty acids in pathogenic cell membranes and exhibits enhanced permeabilization and antimicrobial activity.[34,35] We previously used oriented-sample solid-state NMR on ^{15}N-labeled P1-apo to solve its α-helical structure bound to fluid lipid bilayers.[36−45] However, structural analysis by solid-state NMR is challenged by the intertwined physical and chemical changes that metalation induces in the peptide. Indeed, upon metalation, not only does the ATCUN motif become planar, it also sheds multiple protons from its three backbone nitrogen ligands, yielding nonprotonated amides at positions 2 and 3 (Figure 1a). The fourth ligand, the $N_{\delta1}$ of the H3 side chain, is also nonprotonated in the liganded state while it could be either protonated or deprotonated in the apo-state depending on the pK_a of the side chain. Being nonprotonated in the holo-state, the N_α amides and $N_{\delta1}$ could be hard to detect by standard ^{15}N solid-state NMR experiments since these rely on cross-polarization (CP) from ^{1}H to enhance the sensitivity of nuclei like ^{15}N that have low gyromagnetic ratios.[46,47] Being metalated, the N_α amides and $N_{\delta1}$ could experience significant resonance shifts compared to their standard positions as nonprotonated sites, making assignments difficult.[48−50] Compounding these two challenges is that H3 is juxtaposed with H4, which, as a histidine, could interact with the metal, yielding a modified peptide−metal coordination geometry.[51−53] To identify which nitrogens of H3 and possibly H4 interact with the metal, we develop herein a new NMR experiment that selectively detects and assigns the nonprotonated nitrogens produced and/or shifted by metalation. It relies on magic angle spinning (MAS) to obtain two-dimensional (2D) spectra from unoriented ^{13}C/^{15}N-labeled samples. Combining the NMR data with density functional theory (DFT) calculations, we probe beyond the four predicted nitrogen ligands and unveil structural features of P1 that promote metal binding and bilayer insertion. We reveal a noncanonical arrangement of proximal (H3) and distal (H4) histidines, both in the neutral τ-state, and point at the stabilizing role that a cluster of aromatic residues (F1/F2/H4) could play by mediating cation−π interactions with the metal. Importantly, these findings are applicable to the structures and functions of other ATCUN-containing membrane peptides such as HDPs, amyloids, and neuropeptides that are important to study for applications in the areas of drug-resistant bacteria, neurological disorders, and biomedical imaging.

Figure 2a,b shows the one-dimensional (1D) ^{15}N MAS spectra collected on P1 and P1-Ni^{2+} ^{13}C/^{15}N-labeled at H3. To metalate P1 at pH 7.4, we used diamagnetic Ni^{2+}. This avoids the complications associated with Cu^{2+}, which is paramagnetic and can induce signal broadening and decreased sensitivity for nearby nuclei.[12] These data were obtained using different CP conditions to assess whether nonprotonated nitrogens could be efficiently detected under conventional CP-MAS. CP efficiency highly depends on the strength of ^{1}H−^{15}N dipolar couplings. Due to longer ^{15}N/^{1}H distances, nonprotonated nitrogens exhibit much weaker dipolar couplings than protonated nitrogens. Thus, one would expect that using a longer CP contact time (CT) will improve their signals, but the impact of metalation is hard to predict.

In terms of assigning signals in Figure 2a,b as previously determined for proteins, ^{15}N signals near 120 ppm belong to N_α backbone nitrogens while the imidazole nitrogens resonate near ∼250 ppm if they are nonprotonated or in the range of

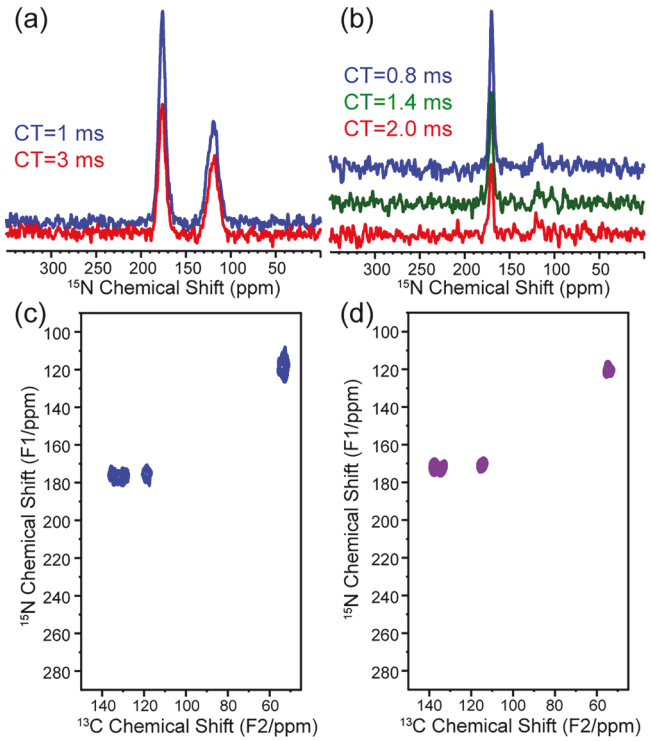

Figure 2. 1D and 2D spectra for ^{15}N/^{13}C-labeled H3-P1 in the apo-state and holo-state (Ni^{2+}-bound). The peptide was first detected by ^{15}N CP/MAS in the apo-state (a) and holo-state (b) using the indicated contact times (CTs). Next, the 2D ^{15}N−^{13}C z-filtered TEDOR correlation spectroscopy was applied to the apo-state (c) and holo-state (d). The pulse sequence is displayed in Figure S1.

150−190 ppm when protonated.[54−56] Given the data in Figure 2a,b, the ^{15}N H3-N_α signal of P1 is significantly weakened in the presence of Ni^{2+}, consistent with the prediction that it loses its bonded proton to chelate Ni^{2+}. Interestingly, a longer CT does not improve the intensity of this nonprotonated N_α. However, it greatly decreases the signals from the imidazole nitrogens near 170 ppm. This effect, which occurs whether the peptide is metalated or not, is stronger for the holo-state, suggesting that the ^{1}H $T_{1\rho}$ shortens significantly upon Ni^{2+}-binding. This may be due to experimental conditions associated with solid-state NMR (e.g., similar spin temperature and $T_1/T_{1\rho}$ for all protons in metalated samples due to fast spin diffusion and spinning speeds not fast enough to average ^{1}H−^{1}H dipolar couplings).[57] The lack of ^{15}N-imidazole peaks above 200 ppm shows that both imidazole nitrogens of H3 are protonated in P1-apo, and thus H3 is charged (biprotonated state). In the case of P1-Ni^{2+} (Figure 2b), the resonances of the imidazole mirror that of the apo-state, but concluding that H3 is charged in the holo-state contradicts the expectation that it is neutral (τ-state) and binds the metal using the nonprotonated $^{15}N_{\delta1}$ (Figure 1a). This led us to hypothesize that Ni^{2+} shifts the resonance of the nonprotonated and liganded $^{15}N_{\delta1}$, inadvertently placing it in the region usually reserved for protonated imidazole nitrogens in metal-free proteins. Next, we used 2D experiments with the aim of assigning the protonation states of the $N_{\delta1}/N_{\varepsilon2}$ imidazole nitrogens and determining whether H3 is neutral and bound to Ni^{2+}.

As a first step to assigning the signals of H3 in P1-Ni^{2+}, we performed the z-filtered transferred-echo-double-resonance

https://doi.org/10.1021/acs.jpclett.1c00636
J. Phys. Chem. Lett. 2021, 12, 4392−4399

(TEDOR) pulse sequence shown in Figure S1.[56,58] Advantageously, this experiment indirectly detects ^{15}N through ^{13}C. This improves sensitivity in two ways. First, ^{13}C is more sensitive than ^{15}N due to its higher gyromagnetic ratio. Second, in contrast to conventional 2D $^{15}N-^{13}C$ correlation experiments,[48−50] this scheme directly cross-polarizes ^{13}C rather than ^{15}N. Thus, even if nonprotonated, ^{15}N sites bound to ^{13}C can be indirectly observed via ^{13}C. Figure S2 displays the z-filtered TEDOR data collected on the isolated amino acid histidine. All peaks can be assigned as well as the chemical states (i.e., charged vs neutral form, π- vs τ-tautomer) adopted by the histidine side chain.

Figure 2c,d shows the spectra obtained when the z-filtered TEDOR sequence is performed on $^{13}C/^{15}N$-labeled H3-P1 in the apo- and holo-states. As for the ^{15}N 1D CP-MAS data, the apo- and holo-states are highly similar and confirm that the H3 side chain of P1-apo is charged. For P1-Ni^{2+}, in contrast to the 1D spectrum (Figure 2b), the 2D TEDOR (Figure 2d) exhibits an intense $^{15}N/^{13}C$ crosspeak at (∼120, ∼55) ppm for H3-N_α. This confirms the sensitivity enhancement of this experiment for nonprotonated N_α nitrogens, as previously reported.[56,58,59] However, these data are inadequate to assign the protonation state of the $N_{\delta1}/N_{\varepsilon2}$.

We similarly collected z-filtered TEDOR data on $^{13}C/^{15}N$-labeled H4-P1 in the apo- and holo-states (Ni^{2+} bound) (Figure S3). The H4 side chain in P1-apo shows the deprotonated ^{15}N signals at ∼250 ppm for the neutral state. It likely populates both neutral states, the τ- and π-tautomers, since two crosspeaks exist near 250 ppm (Figure S3a). Upon Ni^{2+}-binding, a single, sharp crosspeak remains at (∼250, ∼138) ppm (Figure S3b). Given this resonance pattern, H4 stabilizes into the τ-state in P1-holo (the π-state would require a resonance near (250, 120) ppm for the $C_{\delta2}$,[60] but such signal is lacking). The resonances in Figure S3b are annotated accordingly.

The finding that in P1-holo, H4, the side chain neighboring H3, boasts the spectral features associated with the neutral τ-state while H3 lacks them begs the question that H4 could play a direct role in coordinating the metal ion. However, this is unlikely since the ^{15}N resonances for H4 in the τ-state do not shift upon metal-coordination to P1. Instead, the aforementioned hypothesis that Ni^{2+}-binding to the H3 side chain results in a major upfield chemical shift change is more probable. To verify this hypothesis, which requires showing that the $N_{\delta1}$ of H3 is nonprotonated and liganded in P1-holo, we developed a new NMR experiment.

The new NMR pulse sequence designed for this work is presented in Figure S1. It is novel in two ways: (i) it is selective to nonprotonated ^{15}N sites; (ii) it adds to the z-filter of the TEDOR experiment a dipolar recoupling scheme selected to achieve efficient dipolar recoupling. More specifically, it relies on a transverse relaxation T_2-dephasing period to recouple $^{15}N-^{1}H$ dipolar couplings and uses the rotary resonance condition[61,62] over other schemes[63−68] to maximize the difference between the protonated and nonprotonated nitrogen sites. Additional details about the setup of this experiment and its performance on the amino acid histidine are given in the Supporting Information.

Figure 3a shows the z-filtered T_2-dephased TEDOR $^{15}N-^{13}C$ correlation spectrum for $^{13}C/^{15}N$-labeled H3-P1-Ni^{2+}. The crosspeak at (118.9, 54.8) ppm can readily be assigned to the $C_\alpha-N_\alpha$ correlation. Compared to Figure 2d,

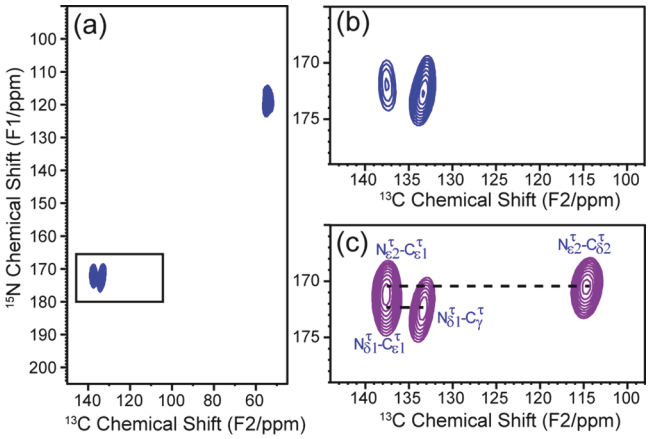

Figure 3. $^{15}N-^{13}C$ correlation spectra for selective detection of nonprotonated nitrogens in $^{15}N/^{13}C$-labeled H3-P1-Ni^{2+}. (a) The z-filtered TEDOR pulse sequence was modified with a T_2-dephasing period of 1.125 ms to selectively detect the nonprotonated ^{15}N sites. (b) The imidazole region from (a) is enlarged. (c) The corresponding region from the z-filtered TEDOR experiment (Figure 2d) shows signals from both the protonated and nonprotonated nitrogens. Comparison of the spectra selective (b) and nonselective (c) to nonprotonated nitrogens makes the indicated assignments possible. The loss of chemical shift dispersion between protonated and nonprotonated nitrogen sites in the holo-state is discussed in the main text and Supporting Information.

the $^{15}N/^{13}C$ crosspeak at (170.7, 114.9) ppm is completely gone and thus belongs to a protonated imidazole ^{15}N. In contrast, the resonances at (172.1, 137.5) ppm and (172.4, 133.3) ppm remain, indicating that they are associated with a nonprotonated imidazole ^{15}N. Thus, the H3 side chain in P1-holo is neutral even though its ^{15}N signals resonate below 200 ppm. Like H4 in P1-Ni^{2+} (Figure S3b), the carbon resonance pattern for H3 is characteristic of the τ-state. The spectrum in Figure 3c is annotated accordingly.

Importantly, the spectral similarities exhibited by H3 in P1 and P1-Ni^{2+} conceal the chemical changes occurring at the $N_{\delta1}$. While it resonates near 170 ppm whether Ni^{2+} is present or not, it is protonated in the former and nonprotonated in the latter. Under metal-free conditions, the nonprotonated state resonates near 250 ppm.[54−56] Thus, the single act of adding Ni^{2+} to P1 induces an 80 ppm upfield shift of the H3-$N_{\delta1}$ resonance compared to its standard position. This remarkable chemical shift perturbation (CSP) is not observed for the H4-$N_{\delta1}$. This clearly establishes the H3-$N_{\delta1}$ as the imidazole nitrogen that chelates Ni^{2+} in P1 and confirms the hypothesis stated above. Notably, Figure 3 shows that the compensatory CSP effects induced by simultaneous metalation and deprotonation apply to not only the H3-$N_{\delta1}$ but also the H3-N_α. The assignment issues resulting from the loss of chemical shift dispersion between protonated and nonprotonated underscore the value of the T_2-dephased TEDOR to decrowd the NMR data. To our knowledge, Figure 3c provides the first assigned 2D $^{13}C/^{15}N$ correlation spectrum for a metal−liganded histidine in an ATCUN-peptide. Structurally, it establishes the tautomeric state of the side chain, the identity of the chelating imidazole nitrogen, and the coordination geometry of the metal-binding motif within the peptide.

Next, we investigated the peptide simultaneously bound to the metal ion and hydrated lipid bilayers. Figures S4−S6

https://doi.org/10.1021/acs.jpclett.1c00636
J. Phys. Chem. Lett. 2021, 12, 4392−4399

Table 1. Selected ATCUN-Containing Membrane-Interacting Peptides That Bind Ni^{2+}/Cu^{2+} and Have Amino Terminal Regions Enriched in Aromatic Residues (Highlighted in Bold)[a]

name	sequence	ref
	Host Defense Peptides (HDPs)	
piscidin 1 (hybrid striped bass)	**FFHHI**FRGIVHVGKTIHRLVTG	24,25, 34, 35
piscidin 3 (hybrid striped bass)	**FIHHI**FRGIVHAGRSIGRFLTG	24, 25, 34, 35
piscidin 4 (tilapia)	**FIHHI**IGGLFSAGKAIHRLIRRRRR	97
gaduscidin (Atlantic cod)	**FIHHI**IGWISHGVRAIHRAIHG	98
hepcidin-25 (human)	DT**HF**PICIFCCGCCHRSKCGMCCKT	99
histatin-8 (human)	K**FH**EKHHSHRGY	100
	β-Amyloid Peptides	
$A\beta_{4-42}$	**FRH**DSGYEVHHQKLVFFAEDVGSNKGAIIGLMVGGVVIA	85, 93
$A\beta_{11-23}$	EV**HH**QKLVFFAED	89
	Neuropeptides	
neuromedin C	GN**HW**AVGHLM	12, 95
YYH-octreotide	**YYH**-FCFWKTCT[b]	96

[a]Additional ATCUN-containing HDPs are listed in Table S3. [b]D-Residues are present at positions 1 and 4 of octreotide. The YYH motif was added to the neuropeptide for PET imaging with ^{64}Cu.

compare the spectra obtained for the $^{15}N/^{13}C$-labeled H3-P1 and H4-P1 peptides (Figure 2a,b) to those acquired when the peptides are metalated and bound to lipids. Due to the dilution of the peptide by the lipid and water, more scans were collected than for the powder form. Despite this lower sensitivity, the same spectral features (e.g., resonance positions) apply whether the lipids are present or not. Strikingly, metalation of the peptides with paramagnetic Cu^{2+} dramatically knocks out the signal of the H3 side chain while this effect does not apply to H4. Thus, the lipid-containing samples yield 1D data that agree completely with that obtained for the powder form of P1, namely, that only H3 is directly interacting with the metal ion and that the deprotonated nitrogen coordinating the metal resonates in the same region as the biprotonated state of the apo-form. The 2D data obtained on $^{13}C/^{15}N$-labeled H3-P1-apo also agree between the lipid-bound state (Figure S6) and powder form (Figure 2).

A salient feature emerging from comparing the 2D spectra for the apo- and holo-states of P1 is the sharpening of resonances that persists once the peptide becomes metalated (Figure 2 and Figure S3). This occurs for both H3 and H4, suggesting that their conformations become more narrowly defined upon metal binding. This would certainly be the case for H3 given the fact that the side chain is directly engaged in forming the planar coordination geometry for the metal. H3 clearly acts as a proximal histidine for the metal ion. Since H4 also appears to be more organized upon Ni^{2+}-binding, this result indicates that this aromatic residue, characterized as a distal histidine in comparison to the proximal H3, could play a stabilizing role in P1-holo in terms of both metal binding and bilayer insertion. Next, we used DFT to further explore this interesting arrangement of proximal and distal histidines, designating it as noncanonical compared to the canonical arrangement epitomized by heme-containing proteins.

DFT has frequently been leveraged to determine NMR properties of histidine-containing peptides[48,69,70] and elucidate details of histidine-metal interactions[71] including in the context of the ATCUN motif.[72−74] Here, we performed DFT calculations on F1F2H3, the ATCUN motif of P1. Before using DFT to investigate side chains beyond H3 that may be involved in P1-Ni^{2+} interactions, we verified that the methodology could accurately predict the $^{13}C/^{15}N$ chemical shifts observed experimentally for the biprotonated form and τ-state of H3 in P1-apo and P1-holo, respectively. The chemical shifts for these two states are listed in Table S1, while Table S2 provides those for the doubly deprotonated form and π-state. Regarding the biprotonated state observed for the apo-state, DFT correctly predicts that protonated imidazole nitrogens resonate below 200 ppm. For the holo-state with H3 in the τ-state, DFT accurately projects that the nonprotonated, liganded $N_{\delta 1}$ resonates near 170 ppm. As explained in the Supporting Information, the shifts predicted for the other three protonation state of metalated H3 are not consistent with the experimental data.

Having benchmarked our DFT calculations on FFH-apo/holo, we then simulated the pentapeptide FFHHI-Ni^{2+}. The goal was to scrutinize how side chains besides the metal-coordinating H3 could contribute to stabilizing the metal ion. H4 was included given its electron-rich aromatic structure and the experimental result that its side chain conformation becomes better defined in the holo-state. The fifth residue was appended to allow the peptide to develop α-helical content beyond the ATCUN motif. The energetically most favored structure (Figure 1b) features H3 as the direct metal−ligand, while H4 lies ∼6 Å below the coordination plane, next to and coplanar with F1. Thus, the DFT-optimized structure reflects the NMR result that H3 and H4 act as a noncanonical pair of proximal and distal histidines. Interestingly, DFT predicts that F1, F2, and H4 form a cluster of aromatic rings in close proximity to Ni^{2+}, especially in the case of F1 and F2. They sit within 6 Å of the metal ion, making them good candidates for significant cation−π interactions.[17] For F2, which lies above the coordination plane, the distance is only 4.40 Å, in the range previously found to produce strong cation−π interactions.[15] Overall, this arrangement of rings in P1 could be stabilizing to the metal, especially considering the bilayer environment where the peptide acts biologically.

In examining whether the cation−π interactions identified in P1 constitute a biophysical characteristic that could be relevant to the structures and functions of other biologically important peptides, we note a broad range of peptide classes that like P1 exhibit the following three traits: (i) demonstrated ability to coordinate Cu^{2+}/Ni^{2+} via an ATCUN-motif; (ii) N-terminal regions rich in aromatic residues; (iii) documented interactions with membranes. Table 1 features members from the most notable families, spanning anti-infective HDPs,[34,75,76] amyloid

https://doi.org/10.1021/acs.jpclett.1c00636
J. Phys. Chem. Lett. 2021, 12, 4392−4399

peptides involved in neurological disorders,[49,50,77−79] and neuropeptides essential to neural function.[12,15] The HDP category includes other piscidins such as P3 and TP4.[34,35,43,74,80] Notably, H4 is highly conserved in the piscidin family. So is a phenylalanine at position 1 and/or position 2.[27,81] Histatins from human saliva are among the most widely known ATCUN-containing host defense metallopeptides. Several members such as histatin-8 contain aromatic rich amino-terminal regions.[82−84] Given their high biocompatibility, histatins have been considered for a wide range of biomedical applications, including oral rinses to fight periodontal diseases and antimicrobial treatments to treat chronic lung infections at a lower risk of resistance than with conventional antibiotics.[84] Next, Table 1 features amyloid Aβ derivatives that are involved in the pathology of Alzheimer's disease (AD). The full length Aβ_{1-42} peptide and some of its truncated forms can bind to two Cu^{2+} ions using non-ATCUN binding sites, enabling them to form damaging radicals.[85−88] Their metalation state and aromatic content modulate their ability to aggregate into oligomers that are membrane disruptive and toxic.[88−92] Removal of the first three residues from Aβ_{1-42} generates the ATCUN-containing fragment Aβ_{4-42}, one of the most abundant Aβ species in the human brain.[85,93] In the aggregated state, Aβ_{4-42} induces neuron loss.[93] However, tightly bound to Cu^{2+}, its redox-silent ATCUN motif FRH stabilizes the ion and prevents it from forming radicals.[85] This has led to the notion that Aβ_{4-42} could play a protective role by scavenging Cu^{2+} in synapses.[85] Investigations are ongoing regarding the use of ATCUN peptides as Cu^{2+}-chelating therapeutics for AD.[94] Finally, neuropeptides are listed in Table 1. In the case of neuromedin C, metalation of its ATCUN motif alters its structure, which is expected to impact its membrane and receptor interactions and thus its role in neurotransmission.[12,95] Spectroscopic studies of metalated neuromedin C point at possible cation−π interactions involving a tryptophan at position 4.[15] YYH-octreotide is an analog of the membrane-binding neuropeptide somatostatin whose receptors are overexpressed in several types of tumors. Via its redox-silent YYH ACTUN motif, it binds very stably to the radionuclide ^{64}Cu, making it an excellent agent to image tumors via positron emission tomography (PET).[96] Using bulky residues at positions 1 and 2 of the ATCUN motif helped stabilize the holo-state for *in vivo* applications. Overall, the broader implication emerging from these examples is that cation−π interactions could represent a structural feature applicable to a broad range of ATCUN-containing membrane peptides. An intriguing consideration for future studies of these peptides would be to investigate whether cation−π interactions influence the strength of their binding affinity to Cu^{2+} and redox capability.

Conclusion. To our knowledge, this thorough investigation of H3 and H4 in P1 and P1-Ni^{2+} demonstrates for the first time that H3 and H4 behave as a noncanonical pair of proximal and distal histidines. DFT identifies a model where the aromatic rings of F1, F2, and H4 are within reach of the metal ion to establish favorable cation−π interactions. Overall, these structural studies help explain how P1, a peptide lacking tertiary structure, inserts metal ions into bilayers, leading to chemical and physical damage and enhanced membrane and antimicrobial activity.[34,35] The stabilizing role of aromatic side chains in metalated membrane peptides has relevance to other aromatic-rich, ATCUN-containing peptides that act at biological membranes. These include a wide range of HDPs, amyloid peptides, and neuropeptides. The biophysical and structural principles learned from this study could help design novel compounds optimized for a wide variety of biochemical, biophysical, and biomedical applications. This is timely given that the field of peptide-based therapeutics and biomedical materials is expanding to meet urgent needs in the areas of drug-resistant pathogens, neurological disorders, and biomedical imaging.

■ ASSOCIATED CONTENT

Supporting Information

The Supporting Information is available free of charge at https://pubs.acs.org/doi/10.1021/acs.jpclett.1c00636.

Materials and NMR experimental details; DFT calculations and analyses; 1D ^{15}N CP-MAS spectra of P1 in lipid forms; TEDOR pulse sequence; $^{15}N-^{13}C$ 2D spectra for histidine and H4-P1 in apo- and holo-states; comparison of ^{15}N CP-MAS spectra obtained with direct versus indirect detection; tables of DFT-calculated $^{13}C/^{15}N$ chemical shifts; DFT-optimized geometries of FFH-Ni^{2+} with different H3 protonation states; table of ATCUN-containing HDPs with amino-terminal regions rich in aromatic residues (PDF)

■ AUTHOR INFORMATION

Corresponding Authors

Riqiang Fu − *National High Magnetic Field Laboratory, Tallahassee, Florida 32310, United States;* orcid.org/0000-0003-0075-0410; Email: rfu@magnet.fsu.edu

Myriam L. Cotten − *Department of Applied Science, William & Mary, Williamsburg, Virginia 23185, United States;* orcid.org/0000-0002-6732-1736; Email: mcotten@wm.edu

Authors

Mary T. Rooney − *Department of Applied Science, William & Mary, Williamsburg, Virginia 23185, United States;* orcid.org/0000-0002-5906-1348

Rongfu Zhang − *National High Magnetic Field Laboratory, Tallahassee, Florida 32310, United States; Department of Chemistry and Biochemistry, Florida State University, Tallahassee, Florida 32306, United States*

Complete contact information is available at: https://pubs.acs.org/10.1021/acs.jpclett.1c00636

Author Contributions

R.F. and M.L.C. planned this project, with M.L.C. providing a backdrop question about how the histidines of the peptide interact with the metal. M.L.C. and M.T.R. made the samples. R.F. designed the new NMR experiment. R.F. and R.Z. collected the solid-state NMR. M.L.C. and R.F. analyzed the NMR data, with M.L.C. identifying the upfield shift of the liganded side chain nitrogen. M.T.R. performed the DFT calculations. R.F. and M.L.C. led the writing of the manuscript, with M.T.R. drafting the DFT section and all authors providing input.

Notes

The authors declare no competing financial interest.

■ ACKNOWLEDGMENTS

All NMR experiments were carried out at the National High Magnetic Field Laboratory supported by the NSF Cooperative

Agreement DMR-1644779 and the State of Florida. M.L.C. acknowledges support from the National Science Foundation (Grant MCB 1716608). The authors acknowledge William & Mary Research Computing for providing computational resources and technical support that have contributed to the results reported within this paper.

REFERENCES

(1) Waldron, K. J.; Rutherford, J. C.; Ford, D.; Robinson, N. J. Metalloproteins and metal sensing. *Nature* **2009**, *460*, 823−830.
(2) Hosler, J. P.; Ferguson-Miller, S.; Mills, D. A. Energy transduction: proton transfer through the respiratory complexes. *Annu. Rev. Biochem.* **2006**, *75*, 165−87.
(3) Lu, Y.; Yeung, N.; Sieracki, N.; Marshall, N. M. Design of functional metalloproteins. *Nature* **2009**, *460*, 855−62.
(4) Bertini, I.; Luchinat, C.; Parigi, G.; Pierattelli, R. Perspectives in paramagnetic NMR of metalloproteins. *Dalton Trans* **2008**, 3782−90.
(5) Nastri, F.; D'Alonzo, D.; Leone, L.; Zambrano, G.; Pavone, V.; Lombardi, A. Engineering Metalloprotein Functions in Designed and Native Scaffolds. *Trends Biochem. Sci.* **2019**, *44*, 1022−1040.
(6) Maiti, B. K.; Govil, N.; Kundu, T.; Moura, J. J. G. Designed Metal-ATCUN Derivatives: Redox- and Non-redox-Based Applications Relevant for Chemistry, Biology, and Medicine. *iScience* **2020**, *23*, 101792.
(7) Harford, C.; Sarkar, B. Amino Terminal Cu(II)- and Ni(II)-Binding (ATCUN) Motif of Proteins and Peptides: Metal Binding, DNA Cleavage, and Other Properties. *Acc. Chem. Res.* **1997**, *30*, 123−130.
(8) Gusman, H.; Lendenmann, U.; Grogan, J.; Troxler, R. F.; Oppenheim, F. G. Is salivary histatin 5 a metallopeptide? *Biochim. Biophys. Acta, Protein Struct. Mol. Enzymol.* **2001**, *1545*, 86−95.
(9) Sankararamakrishnan, R.; Verma, S.; Kumar, S. ATCUN-like metal-binding motifs in proteins: identification and characterization by crystal structure and sequence analysis. *Proteins: Struct., Funct., Genet.* **2005**, *58*, 211−21.
(10) Joyner, J. C.; Cowan, J. A. Target-directed catalytic metallodrugs. *Braz. J. Med. Biol. Res.* **2013**, *46*, 465−85.
(11) Alexander, J. L.; Thompson, Z.; Cowan, J. A. Antimicrobial Metallopeptides. *ACS Chem. Biol.* **2018**, *13*, 844−853.
(12) Gasmi, G.; Singer, A.; Forman-Kay, J.; Sarkar, B. NMR structure of neuromedin C, a neurotransmitter with an amino terminal CuII-, NiII-binding (ATCUN) motif. *J. Pept. Res.* **1997**, *49*, 500−9.
(13) Mal, T. K.; Ikura, M.; Kay, L. E. The ATCUN domain as a probe of intermolecular interactions: application to calmodulin-peptide complexes. *J. Am. Chem. Soc.* **2002**, *124*, 14002−3.
(14) Camerman, N.; Camerman, A.; Sarkar, B. Molecular design to mimic the Cu(II) transport site of human serum albumin. The crystal and molecular structure of Cu(II)-glycylglycyl-L-Histidine-Nmethyl amide monoaquo complex. *Can. J. Chem.* **1976**, *54*, 1309−1316.
(15) Yorita, H.; Otomo, K.; Hiramatsu, H.; Toyama, A.; Miura, T.; Takeuchi, H. Evidence for the cation-pi interaction between Cu2+ and tryptophan. *J. Am. Chem. Soc.* **2008**, *130*, 15266−7.
(16) Dougherty, D. A. The cation-π interaction. *Acc. Chem. Res.* **2013**, *46*, 885−93.
(17) Gallivan, J. P.; Dougherty, D. A. Cation-pi interactions in structural biology. *Proc. Natl. Acad. Sci. U. S. A.* **1999**, *96*, 9459−64.
(18) Dougherty, D. A. Cation-pi interactions in chemistry and biology: a new view of benzene, Phe, Tyr, and Trp. *Science* **1996**, *271*, 163−8.
(19) Hu, W.; Lee, K.-C.; Cross, T. A. Tryptophans in Membrane Proteins: Indole Ring Orientations and Functional Implications in the Gramicidin Channel. *Biochemistry* **1993**, *32*, 7035−7047.
(20) Wimley, W. C.; White, S. H. Experimentally determined hydrophobicity scale for proteins at membrane interfaces. *Nat. Struct. Mol. Biol.* **1996**, *3*, 842−848.
(21) Bowie, J. U. Stabilizing membrane proteins. *Curr. Opin. Struct. Biol.* **2001**, *11*, 397−402.
(22) Zhou, H. X.; Cross, T. A. Influences of membrane mimetic environments on membrane protein structures. *Annu. Rev. Biophys.* **2013**, *42*, 361−92.
(23) Sparks, K. A.; Gleason, N. J.; Gist, R.; Langston, R.; Greathouse, D. V.; Koeppe, R. E. 2nd. Comparisons of interfacial Phe, Tyr, and Trp residues as determinants of orientation and dynamics for GWALP transmembrane peptides. *Biochemistry* **2014**, *53*, 3637−45.
(24) Silphaduang, U.; Noga, E. J. Peptide antibiotics in mast cells of fish. *Nature* **2001**, *414*, 268−269.
(25) Noga, E. J.; Silphaduang, U. Piscidins: a novel family of peptide antibiotics from fish. *Drug News Perspect.* **2003**, *16*, 87−92.
(26) Fjell, C. D.; Hiss, J. A.; Hancock, R. E. W.; Schneider, G. Designing antimicrobial peptides: form follows function. *Nat. Rev. Drug Discovery* **2012**, *11*, 37−51.
(27) Portelinha, J.; Duay, S. S.; Yu, S. I.; Heilemann, K.; Libardo, M. D. J.; Juliano, S. A.; Klassen, J. L.; Angeles-Boza, A. M. Antimicrobial Peptides and Copper(II) Ions: Novel Therapeutic Opportunities. *Chem. Rev.* **2021**, *121*, 2648−2712.
(28) Bhattacharjya, S.; Straus, S. K. Design, Engineering and Discovery of Novel α-Helical and β-Boomerang Antimicrobial Peptides against Drug Resistant Bacteria. *Int. J. Mol. Sci.* **2020**, *21*, 5773.
(29) Mookherjee, N.; Anderson, M. A.; Haagsman, H. P.; Davidson, D. J. Antimicrobial host defence peptides: functions and clinical potential. *Nat. Rev. Drug Discovery* **2020**, *19*, 311−332.
(30) Wang, G. Human antimicrobial peptides and proteins. *Pharmaceuticals* **2014**, *7*, 545−94.
(31) Hancock, R. E. W.; Sahl, H. G. Antimicrobial and host-defense peptides as new anti-infective therapeutic strategies. *Nat. Biotechnol.* **2006**, *24*, 1551−1557.
(32) Conlon, J. M.; Mechkarska, M.; Lukic, M. L.; Flatt, P. R. Potential therapeutic applications of multifunctional host-defense peptides from frog skin as anti-cancer, anti-viral, immunomodulatory, and anti-diabetic agents. *Peptides* **2014**, *57*, 67−77.
(33) van Dijk, A.; Hedegaard, C. J.; Haagsman, H. P.; Heegaard, P. M. H. The potential for immunoglobulins and host defense peptides (HDPs) to reduce the use of antibiotics in animal production. *Vet. Res.* **2018**, *49*, 68.
(34) Libardo, M. D. J.; Bahar, A. A.; Ma, B.; Fu, R.; McCormick, L. E.; Zhao, J.; McCallum, S. A.; Nussinov, R.; Ren, D.; Angeles-Boza, A. M.; Cotten, M. L. Nuclease activity gives an edge to host-defense peptide piscidin 3 over piscidin 1, rendering it more effective against persisters and biofilms. *FEBS J.* **2017**, *284*, 3662−3683.
(35) Paredes, S. D.; Kim, S.; Rooney, M. T.; Greenwood, A. I.; Hristova, K.; Cotten, M. L. Enhancing the membrane activity of Piscidin 1 through peptide metallation and the presence of oxidized lipid species: Implications for the unification of host defense mechanisms at lipid membranes. *Biochim. Biophys. Acta, Biomembr.* **2020**, *1862*, 183236.
(36) Chekmenev, E. Y.; Jones, S. M.; Nikolayeva, Y. N.; Vollmar, B. S.; Wagner, T. J.; Gor'kov, P. L.; Brey, W. W.; Manion, M. N.; Daugherty, K. C.; Cotten, M. High-field NMR studies of molecular recognition and structure-function relationships in antimicrobial piscidins at the water-lipid bilayer interface. *J. Am. Chem. Soc.* **2006**, *128*, 5308−5309.
(37) Chekmenev, E. Y.; Vollmar, B. S.; Forseth, K. T.; Manion, M. N.; Jones, S. M.; Wagner, T. J.; Endicott, R. M.; Kyriss, B. P.; Homem, L. M.; Pate, M.; He, J.; Raines, J.; Gor'kov, P. L.; Brey, W. W.; Mitchell, D. J.; Auman, A. J.; Ellard-Ivey, M.; Blazyk, J.; Cotten, M. Investigating molecular recognition and biological function at interfaces using piscidins, antimicrobial peptides from fish. *Biochim. Biophys. Acta, Biomembr.* **2006**, *1758*, 1359−1372.
(38) Fu, R.; Truong, M.; Saager, R. J.; Cotten, M.; Cross, T. A. High Resolution Heteronuclear Correlation Spectroscopy in Solid State NMR of Aligned Samples. *J. Magn. Reson.* **2007**, *188*, 41−48.
(39) Fu, R.; Gordon, E. D.; Hibbard, D. J.; Cotten, M. High resolution heteronuclear correlation NMR spectroscopy of an antimicrobial peptide in aligned bilayers at high magnetic field:

https://doi.org/10.1021/acs.jpclett.1c00636
J. Phys. Chem. Lett. 2021, 12, 4392−4399

peptide-water interactions at the water-bilayer interface. *J. Am. Chem. Soc.* **2009**, *131*, 10830−10831.
(40) Chekmenev, E.; Vollmar, B.; Cotten, M. Can antimicrobial peptides scavenge around a cell in less than a second? *Biochim. Biophys. Acta, Biomembr.* **2010**, *1798*, 228−234.
(41) De Angelis, A. A.; Grant, C. V.; Baxter, M. K.; McGavin, J. A.; Opella, S. J.; Cotten, M. L. Amphipathic Antimicrobial Piscidin in Magnetically Aligned Lipid Bilayers. *Biophys. J.* **2011**, *101*, 1086−1094.
(42) Perrin, B. S., Jr.; Tian, Y.; Fu, R.; Grant, C. V.; Chekmenev, E. Y.; Wieczorek, W. E.; Dao, A. E.; Hayden, R. M.; Burzynski, C. M.; Venable, R. M.; Sharma, M.; Opella, S. J.; Pastor, R. W.; Cotten, M. L. High-resolution structures and orientations of antimicrobial peptides piscidin 1 and piscidin 3 in fluid bilayers reveal tilting, kinking, and bilayer immersion. *J. Am. Chem. Soc.* **2014**, *136*, 3491−3504.
(43) Hayden, R. M.; Goldberg, G. K.; Ferguson, B. M.; Schoeneck, M. W.; Libardo, M. D.; Mayeux, S. E.; Shrestha, A.; Bogardus, K. A.; Hammer, J.; Pryshchep, S.; Lehman, H. K.; McCormick, M. L.; Blazyk, J.; Angeles-Boza, A. M.; Fu, R.; Cotten, M. L. Complementary Effects of Host Defense Peptides Piscidin 1 and Piscidin 3 on DNA and Lipid Membranes: Biophysical Insights into Contrasting Biological Activities. *J. Phys. Chem. B* **2015**, *119*, 15235−46.
(44) Comert, F.; Greenwood, A.; Maramba, J.; Acevedo, R.; Lucas, L.; Kulasinghe, T.; Cairns, L. S.; Wen, Y.; Fu, R.; Hammer, J.; Blazyk, J.; Sukharev, S.; Cotten, M. L.; Mihailescu, M. The host-defense peptide piscidin P1 reorganizes lipid domains in membranes and decreases activation energies in mechanosensitive ion channels. *J. Biol. Chem.* **2019**, *294*, 18557−18570.
(45) Mihailescu, M.; Sorci, M.; Seckute, J.; Silin, V. I.; Hammer, J.; Perrin, B. S., Jr.; Hernandez, J. I.; Smajic, N.; Shrestha, A.; Bogardus, K. A.; Greenwood, A. I.; Fu, R.; Blazyk, J.; Pastor, R. W.; Nicholson, L. K.; Belfort, G.; Cotten, M. L. Structure and Function in Antimicrobial Piscidins: Histidine Position, Directionality of Membrane Insertion, and pH-Dependent Permeabilization. *J. Am. Chem. Soc.* **2019**, *141*, 9837−9853.
(46) Pines, A.; Waugh, J. S.; Gibby, M. G. Proton-enhanced nuclear induction spectroscopy - method for high-resolution NMR of dilutie spins in solids. *J. Chem. Phys.* **1972**, *56*, 1776−1777.
(47) Schaefer, J.; Stejskal, E. O. C-13 nuclear magnetic-resonance of polymers spinning at magic angle. *J. Am. Chem. Soc.* **1976**, *98*, 1031−1032.
(48) Zhou, L.; Li, S.; Su, Y.; Yi, X.; Zheng, A.; Deng, F. Interaction between Histidine and Zn(II) Metal Ions over a Wide pH as Revealed by Solid-State NMR Spectroscopy and DFT Calculations. *J. Phys. Chem. B* **2013**, *117*, 8954−8965.
(49) Parthasarathy, S.; Yoo, B.; McElheny, D.; Tay, W.; Ishii, Y. Capturing a Reactive State of Amyloid Aggregates: NMR-based Characterization of Copper-Bound Alzheimer Disease Amyloid β-Fibrils in a REDOX Cycle. *J. Biol. Chem.* **2014**, *289*, 9998−10010.
(50) Lee, M.; Wang, T.; Makhlynets, O. V.; Wu, Y.; Polizzi, N. F.; Wu, H.; Gosavi, P. M.; Stohr, J.; Korendovych, I. V.; DeGrado, W. F.; Hong, M. Zinc-binding structure of a catalytic amyloid from solid-state NMR. *Proc. Natl. Acad. Sci. U. S. A.* **2017**, *114*, 6191−6196.
(51) Neupane, K. P.; Aldous, A. R.; Kritzer, J. A. Metal-binding and redox properties of substituted linear and cyclic ATCUN motifs. *J. Inorg. Biochem.* **2014**, *139*, 65−76.
(52) Kozłowski, H.; Bal, W.; Dyba, M.; Kowalik-Jankowska, T. Specific structure−stability relations in metallopeptides. *Coord. Chem. Rev.* **1999**, *184*, 319−346.
(53) Khoury, R. R.; Sutton, G. J.; Ebrahimi, D.; Hibbert, D. B. Formation Constants of Copper(II) Complexes with Tripeptides Containing Glu, Gly, and His: Potentiometric Measurements and Modeling by Generalized Multiplicative Analysis of Variance. *Inorg. Chem.* **2014**, *53*, 1278−1287.
(54) Tan, C.; Chen, Y.; Peng, X.; Chen, Z.; Cai, S.; Cross, T. A.; Fu, R. Revealing weak histidine ^{15}N homonuclear scalar couplings using Solid-State Magic-Angle-Spinning NMR spectroscopy. *J. Magn. Reson.* **2020**, *316*, 106757.
(55) Pelton, J. G.; Torchia, D. A.; Meadow, N. D.; Roseman, S. Tautomeric states of the active-site histidines of phosphorylated and unphosphorylated IIIGlc, a signal-transducing protein from Escherichia coli, using two-dimensional heteronuclear NMR techniques. *Protein Sci.* **1993**, *2*, 543−558.
(56) Miao, Y.; Cross, T. A.; Fu, R. Differentiation of histidine tautomeric states using ^{15}N selectively filtered ^{13}C solid-state NMR spectroscopy. *J. Magn. Reson.* **2014**, *245*, 105−109.
(57) Yilmaz, A.; Yurdakoç, M.; Işik, B. Influence of transition metal ions on NMR proton T1 relaxation times of serum, blood, and red cells. *Biol. Trace Elem. Res.* **1999**, *67*, 187−93.
(58) Jaroniec, C. P.; Filip, C.; Griffin, R. G. 3D TEDOR NMR Experiments for Simultaneous Measurement of Multiple Carbon-Nitrogen Distances in Umiformly ^{13}C,^{15}N-Labeled Solids. *J. Am. Chem. Soc.* **2002**, *124*, 10728−10742.
(59) Shahid, S. A.; Markovic, S.; Linke, D.; van Rossum, B.-J. Assignment and secondary structure of the YadA membrane protein by solid-state MAS NMR. *Sci. Rep.* **2012**, *2*, 803.
(60) Miao, Y.; Fu, R.; Zhou, H. X.; Cross, T. A. Dynamic Short Hydrogen Bonds in Histidine Tetrad of Full-Length M2 Proton Channel Reveal Tetrameric Structural Heterogeneity and Functional Mechanism. *Structure* **2015**, *23*, 2300−2308.
(61) Oas, T. G.; Griffin, R. G.; Levitt, M. H. Rotary resonance recoupling of dipolar interactions in solid-state nuclear magnetic resonance spectroscopy. *J. Chem. Phys.* **1988**, *89*, 692−695.
(62) Takegoshi, K.; Nakamura, S.; Terao, T. ^{13}C-^{1}H dipolar-assisted rotational resonance in magic-angle spinning NMR. *Chem. Phys. Lett.* **2001**, *344*, 631−637.
(63) Gullion, T.; Schaefer, J. Rotational-echo double-resonance NMR. *J. Magn. Reson.* **1989**, *81*, 196−200.
(64) Waugh, J. S. Uncoupling of local field spectra in nuclear magnetic resonance: determination of atomic positions in solids. *Proc. Natl. Acad. Sci. U. S. A.* **1976**, *73*, 1394−1397.
(65) Opella, S. J.; Frey, M. H.; Cross, T. A. Detection of individual carbon resonances in solid proteins. *J. Am. Chem. Soc.* **1979**, *101*, 5856−5857.
(66) Opella, S. J.; Frey, M. H. Selection of nonprotonated carbon resonances in solid-state nuclear magnetic resonance. *J. Am. Chem. Soc.* **1979**, *101*, 5854−5856.
(67) Munowitz, M. G.; Griffin, R. G. Two-dimensional nuclear magnetic resonance in rotating solids: Time reversal effects in chemical shift-dipolar spectra. *J. Chem. Phys.* **1983**, *78*, 613.
(68) Ye, C.; Fu, R.; Hu, J. Z.; Hou, L.; Ding, S. W. Carbon-13 Chemical Shift Anisotropies in Solid Amino Acids. *Magn. Reson. Chem.* **1993**, *31*, 699−704.
(69) Andrade, D.; Colherinhas, G. A_6H polypeptide membranes: Molecular dynamics simulation, GIAO-DFT-NMR and TD-DFT spectroscopy analysis. *J. Mol. Liq.* **2020**, *316*, 113850.
(70) Wei, Y.; de Dios, A. C.; McDermott, A. E. Solid-State ^{15}N NMR Chemical Shift Anisotropy of Histidines: Experimental and Theoretical Studies of Hydrogen Bonding. *J. Am. Chem. Soc.* **1999**, *121*, 10389−10394.
(71) John, L.; Dasan, A.; Joseyphus, R. S.; Joe, I. H. Molecular docking, structural characterization, DFT and cytotoxicity studies of metal(II) Schiff base complexes derived from thiophene-2-carboyaldehyde and L-histidine. *J. Mol. Struct.* **2019**, *1198*, 126934.
(72) Dunbar, R. C.; Martens, J.; Berden, G.; Oomens, J. Binding of Divalent Metal Ions with Deprotonated Peptides: Do Gas-Phase Anions Parallel the Condensed Phase? *J. Phys. Chem. A* **2018**, *122*, 5589−5596.
(73) Mena, S.; Mirats, A.; Caballero, A. B.; Guirado, G.; Barrios, L. A.; Teat, S. J.; Rodriguez-Santiago, L.; Sodupe, M.; Gamez, P. Drastic Effect of the Peptide Sequence on the Copper-Binding Properties of Tripeptides and the Electrochemical Behaviour of Their Copper(II) Complexes. *Chem. - Eur. J.* **2018**, *24*, 5153−5162.
(74) Rai, R. K.; De Angelis, A.; Greenwood, A.; Opella, S. J.; Cotten, M. L. Metal-ion Binding to Host Defense Peptide Piscidin 3 Observed in Phospholipid Bilayers by Magic Angle Spinning Solid-state NMR. *ChemPhysChem* **2019**, *20*, 295−301.

https://doi.org/10.1021/acs.jpclett.1c00636
J. Phys. Chem. Lett. 2021, 12, 4392−4399

(75) Libardo, M. D.; Cervantes, J. L.; Salazar, J. C.; Angeles-Boza, A. M. Improved bioactivity of antimicrobial peptides by addition of amino-terminal copper and nickel (ATCUN) binding motifs. *ChemMedChem* **2014**, *9*, 1892−1901.
(76) Libardo, M. D. J.; Gorbatyuk, V. Y.; Angeles-Boza, A. M. Central Role of the Copper-Binding Motif in the Complex Mechanism of Action of Ixosin: Enhancing Oxidative Damage and Promoting Synergy with Ixosin B. *ACS Infect. Dis.* **2016**, *2*, 71−81.
(77) Niu, Z.; Zhao, W.; Zhang, Z.; Xiao, F.; Tang, X.; Yang, J. The molecular structure of Alzheimer beta-amyloid fibrils formed in the presence of phospholipid vesicles. *Angew. Chem., Int. Ed.* **2014**, *53*, 9294−7.
(78) Gorbenko, G. P.; Kinnunen, P. K. J. The role of lipid−protein interactions in amyloid-type protein fibril formation. *Chem. Phys. Lipids* **2006**, *141*, 72−82.
(79) Qiang, W.; Yau, W. M.; Schulte, J. Fibrillation of beta amyloid peptides in the presence of phospholipid bilayers and the consequent membrane disruption. *Biochim. Biophys. Acta, Biomembr.* **2015**, *1848*, 266−276.
(80) Huang, H. N.; Chan, Y. L.; Wu, C. J.; Chen, J. Y. Tilapia Piscidin 4 (TP4) Stimulates Cell Proliferation and Wound Closure in MRSA-Infected Wounds in Mice. *Mar. Drugs* **2015**, *13*, 2813−33.
(81) Raju, S. V.; Sarkar, P.; Kumar, P.; Arockiaraj, J. Piscidin, Fish Antimicrobial Peptide: Structure, Classification, Properties, Mechanism, Gene Regulation and Therapeutical Importance. *Int. J. Pept. Res. Ther.* **2021**, *27*, 91−107.
(82) Troxler, R. F.; Offner, G. D.; Xu, T.; Vanderspek, J. C.; Oppenheim, F. G. Structural relationship between human salivary histatins. *J. Dent. Res.* **1990**, *69*, 2−6.
(83) Edgerton, M.; Koshlukova, S. E.; Lo, T. E.; Chrzan, B. G.; Straubinger, R. M.; Raj, P. A. Candidacidal activity of salivary histatins. Identification of a histatin 5-binding protein on Candida albicans. *J. Biol. Chem.* **1998**, *273*, 20438−47.
(84) Melino, S.; Santone, C.; Di Nardo, P.; Sarkar, B. Histatins: salivary peptides with copper(II)- and zinc(II)-binding motifs: perspectives for biomedical applications. *FEBS J.* **2014**, *281*, 657−72.
(85) Wezynfeld, N. E.; Stefaniak, E.; Stachucy, K.; Drozd, A.; Płonka, D.; Drew, S. C.; Krężel, A.; Bal, W. Resistance of Cu(Aβ4-16) to Copper Capture by Metallothionein-3 Supports a Function for the Aβ4-42 Peptide as a Synaptic Cu(II) Scavenger. *Angew. Chem., Int. Ed.* **2016**, *55*, 8235−8.
(86) Huang, X.; Moir, R. D.; Tanzi, R. E.; Bush, A. I.; Rogers, J. T. Redox-active metals, oxidative stress, and Alzheimer's disease pathology. *Ann. N. Y. Acad. Sci.* **2004**, *1012*, 153−63.
(87) Reybier, K.; Ayala, S.; Alies, B.; Rodrigues, J. V.; Bustos Rodriguez, S.; La Penna, G.; Collin, F.; Gomes, C. M.; Hureau, C.; Faller, P. Free Superoxide is an Intermediate in the Production of H_2O_2 by Copper(I)-Aβ Peptide and O_2. *Angew. Chem., Int. Ed.* **2016**, *55*, 1085−9.
(88) Curtain, C. C.; Ali, F.; Volitakis, I.; Cherny, R. A.; Norton, R. S.; Beyreuther, K.; Barrow, C. J.; Masters, C. L.; Bush, A. I.; Barnham, K. J. Alzheimer's disease amyloid-beta binds copper and zinc to generate an allosterically ordered membrane-penetrating structure containing superoxide dismutase-like subunits. *J. Biol. Chem.* **2001**, *276*, 20466−73.
(89) Pradines, V.; Stroia, A. J.; Faller, P. Amyloid fibrils: modulation of formation and structure by copper(ii). *New J. Chem.* **2008**, *32*, 1189−1194.
(90) Yugay, D.; Goronzy, D. P.; Kawakami, L. M.; Claridge, S. A.; Song, T.-B.; Yan, Z.; Xie, Y.-H.; Gilles, J.; Yang, Y.; Weiss, P. S. Copper Ion Binding Site in β-Amyloid Peptide. *Nano Lett.* **2016**, *16*, 6282−6289.
(91) Genji, M.; Yano, Y.; Hoshino, M.; Matsuzaki, K. Aromaticity of Phenylalanine Residues Is Essential for Amyloid Formation by Alzheimer's Amyloid β-Peptide. *Chem. Pharm. Bull.* **2017**, *65*, 668−673.
(92) Gazit, E. A possible role for π-stacking in the self-assembly of amyloid fibrils. *FASEB J.* **2002**, *16*, 77−83.
(93) Bouter, Y.; Dietrich, K.; Wittnam, J. L.; Rezaei-Ghaleh, N.; Pillot, T.; Papot-Couturier, S.; Lefebvre, T.; Sprenger, F.; Wirths, O.; Zweckstetter, M.; Bayer, T. A. N-truncated amyloid β (Aβ) 4-42 forms stable aggregates and induces acute and long-lasting behavioral deficits. *Acta Neuropathol.* **2013**, *126*, 189−205.
(94) Zhang, Q.; Hu, X.; Wang, W.; Yuan, Z. Study of a Bifunctional Aβ Aggregation Inhibitor with the Abilities of Antiamyloid-β and Copper Chelation. *Biomacromolecules* **2016**, *17*, 661−668.
(95) Polverini, E.; Neyroz, P.; Fariselli, P.; Casadio, R.; Masotti, L. The Effect of Membranes on the Conformation of Neuromedin C. *Biochem. Biophys. Res. Commun.* **1995**, *214*, 663−668.
(96) Miyamoto, T.; Fukino, Y.; Kamino, S.; Ueda, M.; Enomoto, S. Enhanced stability of Cu(2+)-ATCUN complexes under physiologically relevant conditions by insertion of structurally bulky and hydrophobic amino acid residues into the ATCUN motif. *Dalton Trans* **2016**, *45*, 9436−45.
(97) Narayana, J. L.; Huang, H. N.; Wu, C. J.; Chen, J. Y. Efficacy of the antimicrobial peptide TP4 against Helicobacter pylori infection: in vitro membrane perturbation via micellization and in vivo suppression of host immune responses in a mouse model. *Oncotarget* **2015**, *6*, 12936−54.
(98) Portelinha, J.; Heilemann, K.; Jin, J.; Angeles-Boza, A. M. Unraveling the implications of multiple histidine residues in the potent antimicrobial peptide Gaduscidin-1. *J. Inorg. Biochem.* **2021**, *219*, 111391.
(99) Kulprachakarn, K.; Chen, Y. L.; Kong, X.; Arno, M. C.; Hider, R. C.; Srichairatanakool, S.; Bansal, S. S. Copper(II) binding properties of hepcidin. *JBIC, J. Biol. Inorg. Chem.* **2016**, *21*, 329−38.
(100) Houghton, E. A.; Nicholas, K. M. In vitro reactive oxygen species production by histatins and copper(I,II). *JBIC, J. Biol. Inorg. Chem.* **2009**, *14*, 243−251.

https://doi.org/10.1021/acs.jpclett.1c00636
J. Phys. Chem. Lett. 2021, 12, 4392−4399